Journal of Sound and Vibration (2002) **251**(2), 315–327
doi:10.1006/jsvi.2001.3981, available online at http://www.idealibrary.com on IDEAL®

A COUPLED FLUID–STRUCTURE ANALYSIS FOR 3-D INVISCID FLUTTER OF IV STANDARD CONFIGURATION

V. GNESIN

Department of Aerohydromechanics, Institute for Problems in Machinery, Ukrainian National Academy of Sciences, 2/10 *Pozharsky st., Kharkov* 310046, *Ukraine*

AND

R. RZĄDKOWSKI

Institute of Fluid-Flow Machinery, Polish Academy of Sciences, Fiszera 14, *PL* 80-952 *Gdańsk, Poland.*
E-mail: z3@imp.gda.pl
and Polish Naval Academy, Faculty of Mechanical and Electrical Engineering, Poland

(*Received* 24 *October* 2000, *and in final form* 14 *August* 2001)

A three-dimensional non-linear time-marching method and numerical analysis for aeroelastic behaviour of an oscillating blade row is presented. The approach is based on the solution of the coupled fluid–structure problem in which the aerodynamic and structural equations are integrated simultaneously in time. In this formulation of a coupled problem, the interblade phase angle at which a stability (or instability) would occur is a part of the solution. The ideal gas flow through multiple interblade passage (with periodicity on the whole annulus) is described by the unsteady Euler equations in the form of conservative laws, which are integrated by use of the explicit monotonic second order accurate Godunov–Kolgan volume scheme and a moving hybrid H–H (or H–O) grid. The structure analysis uses the modal approach and 3-D finite element model of the blade. The blade motion is assumed to be a linear combination of modes shapes with the modal coefficients depending on time. The influence of the natural frequencies on the aerodynamic coefficient and aeroelastic coupled oscillations for the Fourth Standard Configuration is shown. The stability (instability) areas for the modes are obtained. It has been shown that interaction between modes plays an important role in the aeroelastic blade response. This interaction has an essentially non-linear character and leads to blade limit cycle oscillations.

1. INTRODUCTION

Modern turbomachines operate under very complex regimes where a mixture of subsonic, transonic and supersonic regions coexist. With recent advances in internal compressible flow modelling and increased computational power, it is now possible to undertake both steady and unsteady flow analysis of very complex turbomachinery geometry. The trend for improved gas turbine engine design with higher aerodynamic blade loading and smaller physical size attracts much attention to the aeroelastic behaviour of blades not only in compressors, but also in turbines. Flow-induced blades oscillations of the turbine and compressor can lead to fatigue failures of a construction and so they represent an important problem of reliability, safety, and operating cost.

Aeroelasticity phenomena are characterized by the interaction of fluid and structural domains, most prediction methods tend to treat the two domains separately, and they

0022-460X/02/120315 + 13 $35.00/0

usually assume some critical interblade phase angle for which the flutter analysis is carried out for a single passage.

The undeniable importance of spatial and non-linear effects for practical turbomachinery configurations has led to the development of three-dimensional methods. Since the early 1980s a number of time accurate Euler and Navier–Stokes procedures have been developed to predict blade row unsteady flows in which unsteadiness is caused by aerodynamic disturbances at the inflow or outflow boundaries, relative motions between the blade rows, or blade vibrations. The traditional approach in flutter calculations of bladed disks is based on frequency domain analysis [1, 2], in which the blade motions are assumed to be harmonic functions of time with a constant phase lag between adjacent blades, and the mode shapes and frequencies are obtained from structural computations. This approach ignores the feedback effect of the fluid on the structural vibration.

In recent times, the new approaches based on the simultaneous integration in time of the equations of motion for the structure and the fluid have been developed [3–12]. These approaches are very attractive due to the general formulation of a coupled problem, as the interblade phase angle at which a stability (instability) would occur is a part of the solution.

In the present study, the simultaneous time integration method has been described to calculate the aeroelastic behaviour for a three-dimensional oscillating blade row in transonic gas flow.

2. AERODYNAMIC MODEL

The flow model is described in detail in reference [10]; a brief summary will be given here for the sake of completeness. The 3D transonic flow of an ideal gas through a multipassage blade row is considered. In the general case, the flow is assumed to be a periodic function from blade to blade (in pitchwise direction), so the calculated domain includes all blades of the whole assembly (see Figure 1).

The flow equations will be written for a three-dimensional Cartesian co-ordinate system which is fixed to a rotating blade row. In this case, the conservative form of the unsteady Euler equations is given by [10]

$$\frac{\partial}{\partial t}\int_{\Omega}\mathbf{f}\,\mathrm{d}\Omega+\oint_{\sigma}\mathbf{F}\cdot\mathbf{n}\,\mathrm{d}\sigma+\int_{\Omega}\mathbf{H}\,\mathrm{d}\Omega=0. \tag{1}$$

Here $\mathbf{f}$ is the solution vector, $\mathbf{F}$ is the inviscid flux through the lateral area σ bounding the finite volume Ω, and $\mathbf{H}$ is the source vector which contains the terms due to the rotation of the coordinate system. The above system of equations is completed by the perfect gas equation

$$p=\rho\varepsilon(\chi-1), \tag{2}$$

where χ denotes the ratio of the fluid specific heats and ε is an internal energy of mass unit. The spatial solution domain is discretized by using linear hexahedral elements. Equations (1) and (2) are integrated on a moving H–H (or H–O)–type grid with use of the explicit monotonic second order accuracy Godunov–Kolgan difference scheme.

It is assumed that the unsteady fluctuations in the flow are due to prescribed blade motions, and the flows far upstream and far downstream from the blade row are at most small perturbations of uniform free streams. So the boundary conditions formulation is based on the one-dimensional theory of characteristics, where the number of physical

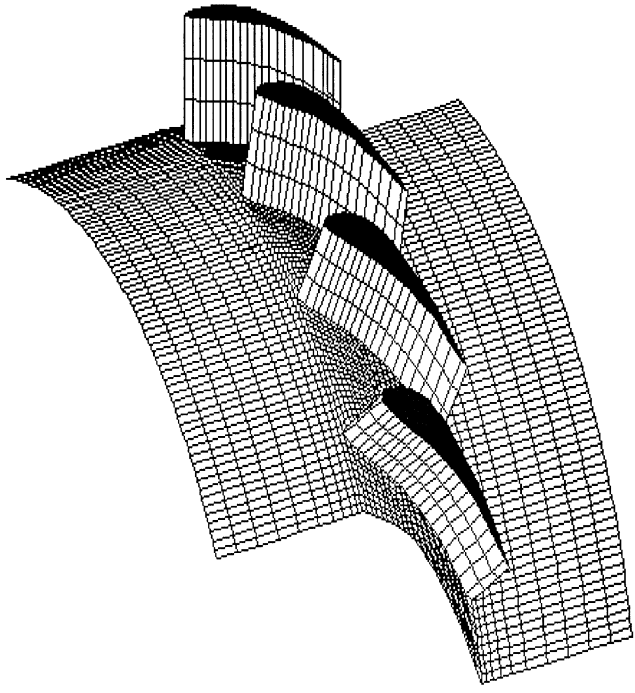

Figure 1. A view of a sector of the whole blade assembly.

boundary conditions depends on the number of characteristics entering the computational domain.

In the general case, when the axial velocity is subsonic at the inlet boundary initial values for total pressure, total temperature and flow angles are used in terms of the rotating frame of reference, while at the outlet boundary only the static pressure has to be imposed. On the blade surface, zero flux is applied across the solid surface (the grid moves with the blade).

In general, computations are made using a number of blades passages equal to the number of blades in the cascade. Periodic conditions are applied at the upper and lower boundaries of the calculated domain at each time moment. However, there are some situations where it is possible to reduce the number of passages used in the calculations. For unsteady flows in which all blades perform harmonic oscillations with a particular mode shape, frequency and a constant interblade phase angle (IBPA) (tuned cascades), the number of blades passages depends on the value of the interblade phase angle. For instance, computations with the phase angle $\delta = \pm 90^\circ$ can be made for four passages. In the time domain method, in which the motion of the blades of a coupled fluid–structure problem is not known in advance, it is necessary to include in the numerical calculations all blade passages. The time step at the coupled calculations is assumed to be constant and is chosen from the stability conditions of the explicit scheme for the fluid model.

3. STRUCTURAL MODEL

The structural model is based on a linear modal model [13], the mode shapes and natural frequencies being obtained via standard FE analysis techniques. Each blade is treated as an individual during the numerical calculations.

The structural part of the aeroelastic equations of motion are uncoupled by using the mode shape matrix. The displacement of each blade can be written as a linear combination of the first N modes shapes with the modal coefficients depending on time,

$$\mathbf{u}(\mathbf{x}, t) = \mathbf{U}(\mathbf{x}, t)\mathbf{q}(t) = \sum_{i=1}^{N} \mathbf{U}_i(\mathbf{x}) q_i(t), \tag{3}$$

where $\mathbf{U}_i(\mathbf{x})$ is the displacement vector corresponding to the ith mode shape and $q_i(t)$ is the modal coefficient of the ith mode.

Function $\mathbf{U}$ satisfies the orthogonality conditions and normalization condition, so the equation of motion of the tuned blades reduces to the set of independent differential equations relatively to modal coefficients of modes shapes:

$$\ddot{q}_i(t) + \omega_i^2 q_i(t) = \lambda_i(t). \tag{4}$$

Recalculation of modal forces λ_i is performed on each iteration (see reference [10]) with use of the instantaneous pressure field calculated for all cells of the blade, in the following way:

$$\lambda_i = \frac{\iint_\sigma p\bar{U}_i \cdot \mathbf{n}^0 \, \mathrm{d}\sigma}{\iiint_v \rho \bar{U}_i^2 \, \mathrm{d}v}. \tag{5}$$

Here the numerator represents the work of pressure forces at the blade displacement in accordance with the ith mode. The pressure p is the function of q_i and $\mathrm{d}q_i/\mathrm{d}t$. The denominator represents the normalizing factor. Having defined the modal coefficients from the set of equations (4), blade displacement and velocity can be obtained in the form of equation (3).

Boundary conditions from the structural and aerodynamic domains are exchanged at each time step and the aerodynamic mesh is moved to follow the structure motion (the partially coupled method). The structural damping is not included here. The scheme used to integrate the structural equations is the same as the scheme used in the flow code. For this scheme the accuracy of the calculations of natural frequencies and mode shapes is sufficient. The integration scheme introduces a damping; this value is very small and was found from calculations done with the aerodynamic forces set to zero.

4. NUMERICAL RESULTS

The numerical calculations have been carried out for the turbine cascade known as the Fourth Standard Configuration, which has been experimentally investigated in the non-rotating annular cascade tunnel in transonic flow [1]. As the first step, the numerical calculations were performed to compare with the experimental ones.

The steady and unsteady predictions have been made on the hybrid H–H-type grid with $10 \times 30 \times 60$ grid points including the moving H-grid (16 points across) near the blade. In order to compare the results for the unsteady flow, the numerical results for the steady flow must be validated, because they are the starting point for the unsteady flow calculations. In Figure 2(a) the calculated and experimental results of steady pressure coefficient are presented and in Figure 2(b) the distribution of the isentropic Mach number along the middle section of the blade is shown. The integers "1" and "2" correspond to the suction and

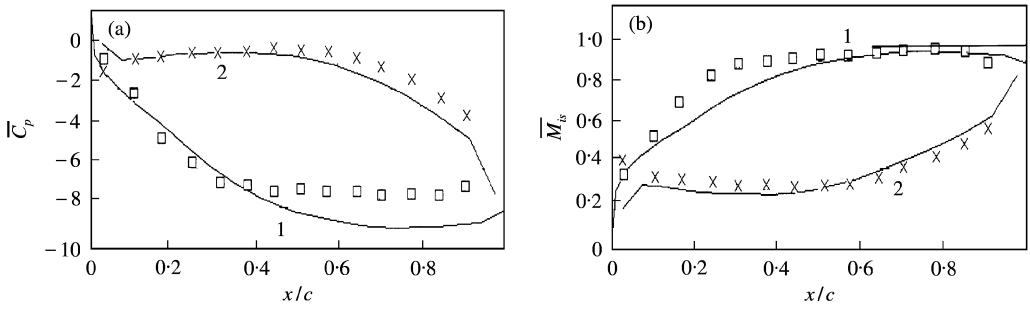

Figure 2. (a) The time-averaged pressure coefficient distribution over the blade chord: 1, suction side; 2, pressure side; □□, pressure side experiment; × ×, suction side experiment. (b) The Mach number distribution over the blade chord: 1, suction side; 2, pressure side; □□, pressure side experiment; × ×, suction side experiment.

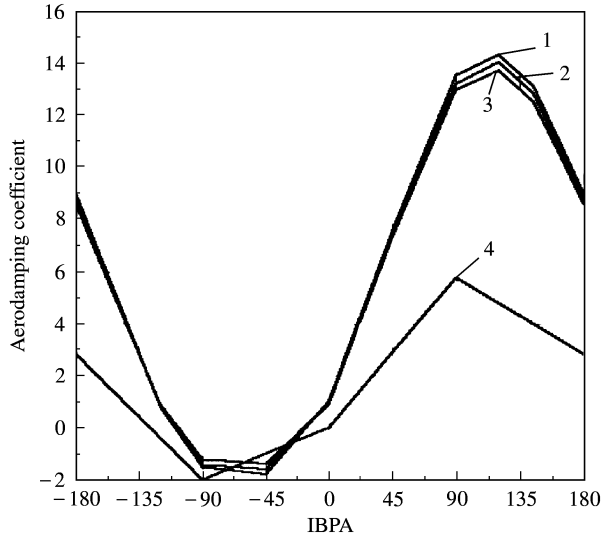

Figure 3. Aerodamping coefficient in dependence of interblade phase angle: 1, casing; 2, mid; 3, hub; 4, experiment.

pressure sides respectively. Agreement between the numerical and experimental results is quite good. The small discrepancies are noticeable near the leading edge at approximately 30% of the chord length on the suction side.

The influence of the interblade phase angle on the aerodamping coefficient for the assumed bending oscillations is shown in Figure 3. Aerodamping coefficient D is equal to the negative work coefficient during one cycle of oscillations. In that figure the numerical calculated aerodamping coefficients in the hub ("1"), middle ("2") and root ("3") sections and the experimental ones ("4") are presented. From these results the strong influence of IBPA is visible. In the range of $-120^\circ < \text{IBPA} < -30^\circ$ the aerodamping coefficients have negative values that correspond to the transfer of energy from the flow to the oscillating blades. The maximum aerodamping coefficient is for IBPA close to 90°. In this case the aerodamping coefficient does not depend on the blade length. The experimental values of the aerodamping coefficient is close to the calculated results although small difference is found in the vicinity of the maximum value of the aerodamping coefficient.

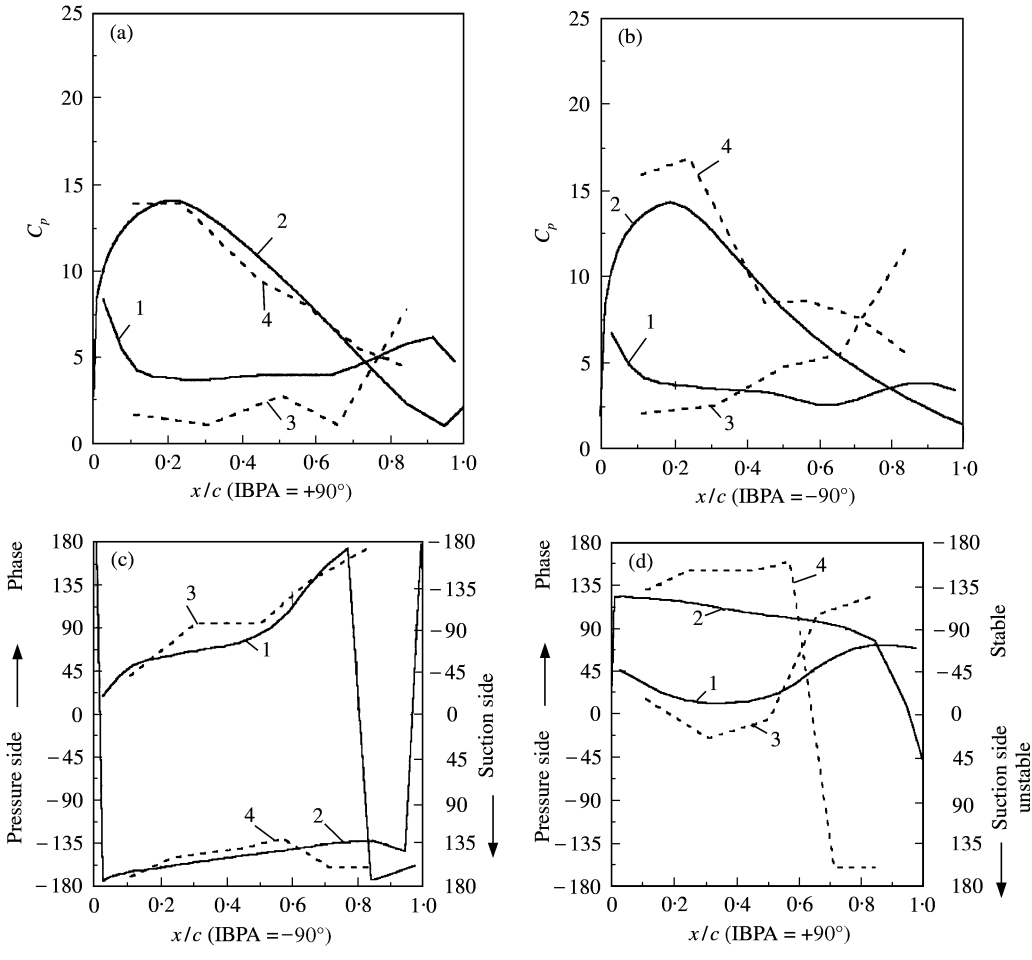

Figure 4. (a, b) The first harmonic unsteady pressure amplitude along the blade chord: 1, pressure side theory; 2, suction side theory; 3, pressure side experiment; 4, suction side experiment. (c, d) The phase distribution along the blade chord: 1, pressure side theory; 2, suction side theory; 3, pressure side experiment; 4, suction side experiment.

A comparison of the calculated and experimental distribution of the first harmonic amplitude and the phase for IBPA of $\pm 90^\circ$ is presented in Figure 4. The agreement is satisfactory. The minimal and maximal values of unsteady pressure occur for in-phase and counter-phase oscillations respectively. The energy exchange between the passing flow and the vibrating blade is defined by the pressure phase shift relative to the blade motion. The positive phase shift on the pressure side and the negative phase shift on the suction side correspond to aerodamping of the system (stability) (see reference [14]).

In the next step of the numerical study the influence of the first four mode shapes on the blade response in the coupled fluid–structure calculations is shown. The mode shapes of the considered blade are presented in Figure 5. The first mode is mainly the bending mode, the second one is the torsional mode, the third and fourth ones are the bending–torsion modes. The natural frequencies are equal to the 150, 750, 900 and 1050 Hz respectively.

Figures 6 and 7 show the aerodamping coefficient versus the interblade phase angle for the first and second natural mode shapes of STC4, respectively, under harmonic oscillations

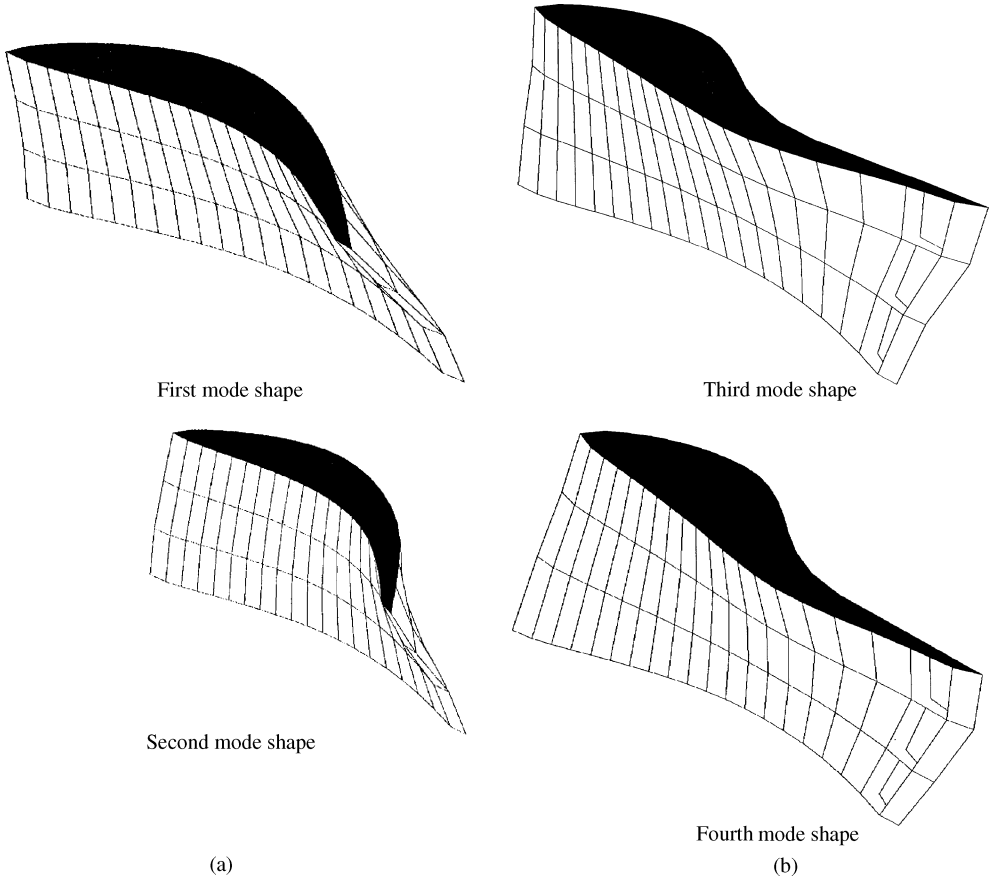

Figure 5. (a) The natural mode shapes of the blade, first mode shape, second mode shape. (b) The natural mode shapes of the blade, third mode shape, fourth mode shape.

with different frequencies (calculated by 3-D flutter aerodynamic model). The negative values of Ψ correspond to the transfer of energy from the flow to the blade (self-excitation), and the positive values correspond to dissipation of an oscillating blade energy to the flow. All curves have the typical sinusoidal forms. It is that the aerodamping grows as the oscillation frequency increases.

It should be pointed out that the oscillations according to the first mode (bending oscillations) are characterized by the negative values of aerodamping coefficient near the IBPA of -90° (see Figure 6), while the oscillations according to the second mode have the self-excitation area near the IBPA of 90° (see Figure 7).

The influence of the phase angle on the sign of the aerodamping coefficient is important for the low modes of vibration and low natural frequencies. It decreases with increase of the mode number and natural frequencies. Aerodamping coefficient grows almost linearly taking positive values over all frequency range except the area of low frequencies ($f < 300$ Hz). Figure 8 shows the areas of possible instability for STC4 (Fourth Standard Configuration). It can be seen that instability of the first mode appears at the phase angle equal to -90° ($f < 150$ Hz) whereas the instability of the second mode appears at phase angle equal to $+90^\circ$ ($f < 250$ Hz). The higher the natural modes are the more stable the cascade is, over the full frequency range.

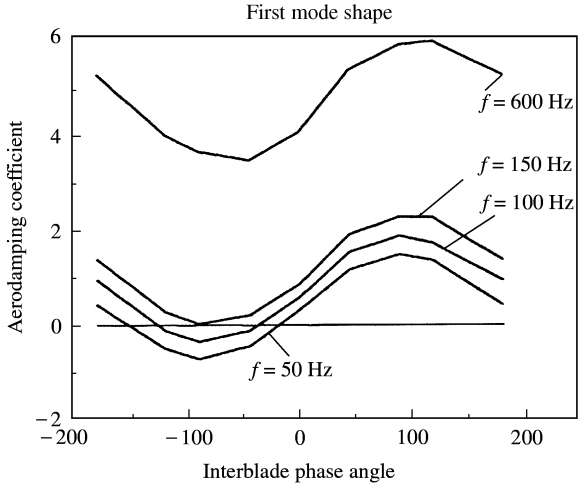

Figure 6. Aerodamping coefficient versus interblade phase angle for the first mode of vibration and different vibration frequencies.

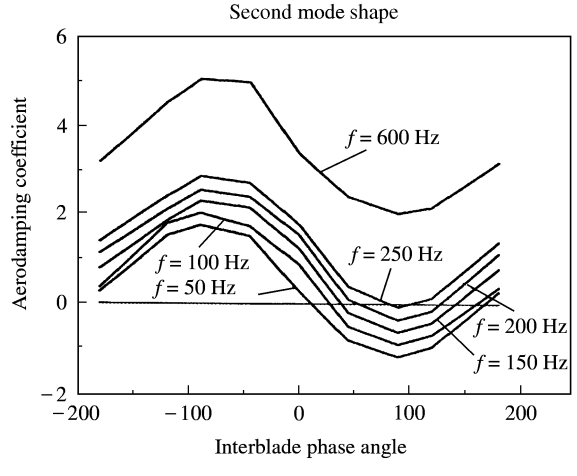

Figure 7. Aerodamping coefficient versus interblade phase angle for the second mode of the vibration and different vibration frequencies.

The sign of the aerodamping coefficient calculated for the harmonic oscillations, may be considered only as a necessary but not sufficient condition for self-excited oscillations. The final estimation of the blade row aeroelastic behaviour may be obtained on the basis of the coupled fluid–structure solution in the time marching algorithm. In this case the blade response is defined not only by the harmonic time history, at which the aerodamping coefficient has been calculated, but also by such parameters which influence the aerodynamic force as the mass flow, the blade mass and the natural frequency of the blade.

All calculations were run from the very beginning for harmonic oscillations until the steady state periodic flow through the vibrating blade row converged. During this time the forced frequencies of harmonic oscillations of each mode were equal to their natural frequencies respectively. After some time moment, named as the start regime, there began

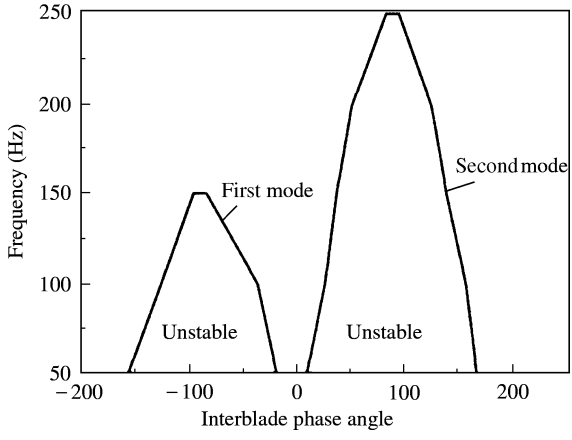

Figure 8. The stability regions for the first and second mode shapes.

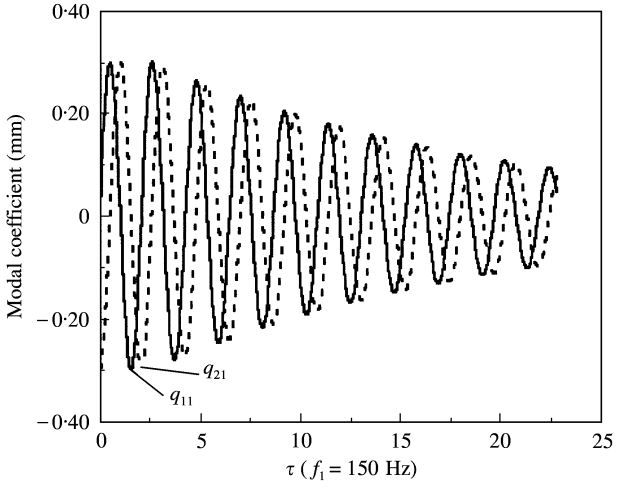

Figure 9. The aeroelastic oscillations of two adjacent blades for the first mode, $t = (\tau/316)$ [s].

the coupled vibrations in which the blade displacements and velocities, and the flow parameters are used as the initial conditions for the coupled time-integration procedure.

One can consider the aeroelastic blade response, vibrating from the beginning at the harmonic oscillations with IBPA of -90°, and next according to fluid–structure interaction.

Figure 9 illustrates the two adjacent blades motion of the first mode with forced frequency 150 Hz. It corresponds to aerodamping coefficient value close to zero (see Figure 6). Here q_{11} and q_{21} denote the modal coefficients for the first and second blade oscillation of the first mode. As can be seen from Figure 9, the blade oscillations are damped with the logarithmic decrement equal to an approximately constant value. It indicates that the blade motion is close to the linear damped oscillations. The blades are fixed at the root, so the root conditions are different from the experiment [1]. This is the reason for the damped oscillations instead of the typical flutter response.

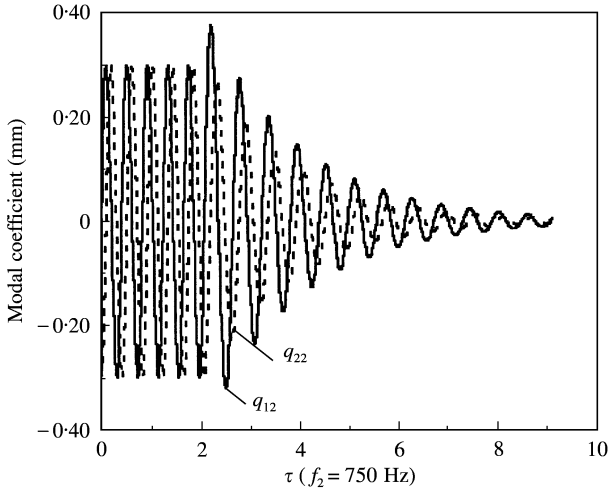

Figure 10. The aeroelastic oscillations of two adjacent blades corresponding to the second mode, $t = (\tau/316)$ [s].

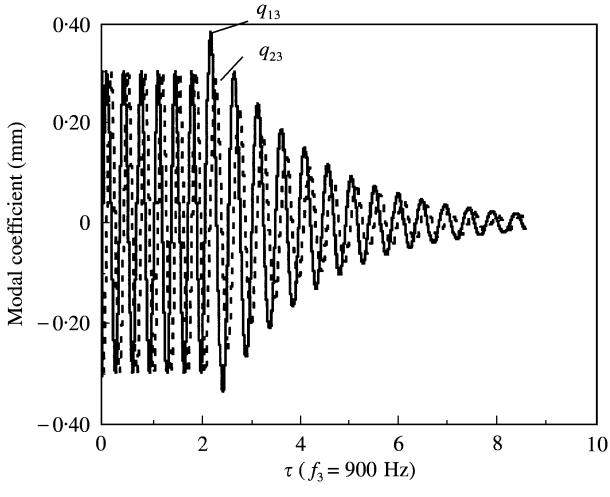

Figure 11. The aeroelastic oscillations of two adjacent blades corresponding to the third mode, $t = (\tau/316)$ [s].

Figure 10 presents the analogous graphs for the two adjacent blades oscillations corresponding to the second mode of vibration, Figure 11 to the third mode and Figure 12 to the fourth mode. For all regimes the oscillations are damped. The higher the natural frequency, the more stable the blade is.

The different character of the blade motion was observed for consideration of the interaction of the natural mode vibrations. Figure 13 shows the blade response at the harmonic oscillations corresponding to the first and second modes. It is clearly observed that response of the blade for the second mode shape decays, but the amplitude of the first mode tends to the approximately constant value, that corresponds to the limit cycle of oscillations. A similar situation is observed for the harmonic oscillation corresponding to the first up to the fourth natural modes. Figures 14 and 15 show the two adjacent blade

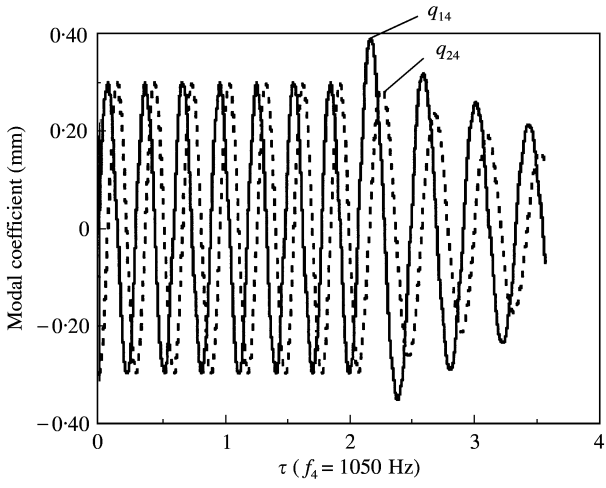

Figure 12. The aeroelastic oscillations of two adjacent blades corresponding to the fourth mode, $t = (\tau/316)$ [s].

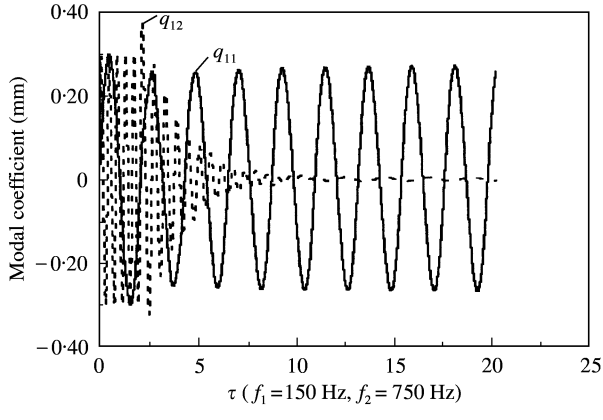

Figure 13. The aeroelastic oscillations of two adjacent blades corresponding to the first and second mode, $t = (\tau/316)$ [s].

response for taking into account the interaction of first, second, third and fourth natural modes at the initial IBPA of $+90^\circ$. Although the aerodamping coefficient at the harmonic oscillation is positive (that corresponds to the stable motion), a transient behaviour is observed and the blades motion changes to the oscillations with the interblade phase angle equalling -90°.

As IBPA of -90° represents an unstable condition for the first mode, the amplitude of the first mode grows approaching the limit cycle of oscillations.

5. CONCLUSIONS

In the present study, the simultaneous time domain method and the modal superposition method have been used to determine the aeroelastic stability of the cascade. The numerical analysis of the influence of natural modes on an aeroelastic blade response for the Fourth

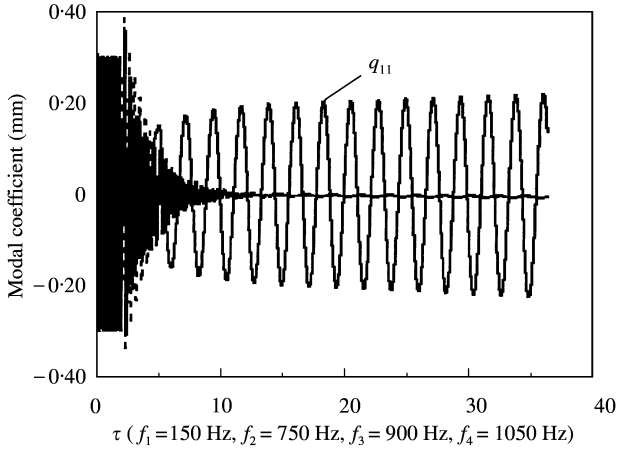

Figure 14. The first blade oscillations by the first, second, third and fourth modes (IBPA of $+90°$), ($t = \tau/316$) [s].

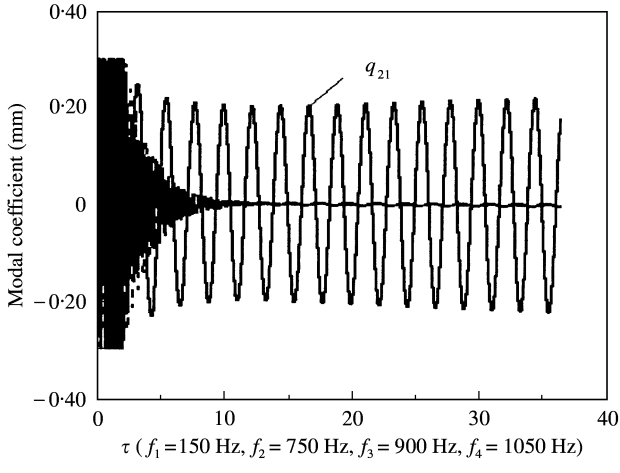

Figure 15. The second blade oscillations by the first, second, third and fourth modes (IBPA of $+90°$), ($t = \tau/316$) [s].

Standard Configuration has been carried out. It has shown that each of the mode shapes oscillations in the range of frequencies $f > 150$ Hz is damped. The interaction between the modes shapes has essentially a non-linear character and leads to limit cycle vibrations (blade auto-oscillations).

The presented time domain method allows a more realistic simulation of the motion of the fluid and the cascade blades that should lead to a better physical understanding.

REFERENCES

1. A. BÖLCS and T. H. FRANSSON 1986 *Communication du LTAT-EPFL Switzerland* 13. Aeroelasticity in turbomachines: comparison of theoretical and experimental cascade results.
2. F. MOYROUD, G. JACQUET-RICHARDE and T. H. FRANSSON 1996 *ASME Paper* 96-*GT*-335, 1–19. A modal coupling for fluid and structure analysis of turbomachines flutter application to a fan stage.

3. M. A. BAKHLE, T. S. R. REDDY and T. G. KEITH 1992 *American Institute of Aeronautics and Astronautics Journal* **30**, 163–170. Time domain flutter analysis of cascades using a full-potential solver.
4. O. O. BENDIKSEN 1998 *Proceedings of ISROMAC-7, The Seventh International Symposium on Transport Phenomena and Dynamics of Rotating Machinery, Honolulu, HI, U.S.A.* February, 22–26. Nonlinear blade vibration and flutter in transonic rotors.
5. O. O. BENDIKSEN 2000 *The Nineth International Symposium of Unsteady Aerodynamics and Aeroelasticity of Turbomachines, Book of Abstracts, Lyon, France, September* 4–8. Transonic bending flutter in rotors and cascades.
6. V. CARSTENS and J. BELZ 2000 *ASME Paper* 2000-*GT*-0381. Numerical investigation of nonlinear fluid–structure interaction in vibrating compressor blades.
7. L. HE 1994 *Journal of Computational Fluid Dynamics* **3**, 217. Integration of 2D fluid/structure coupled systems for calculation of turbomachinery aerodynamic, aeroelastic instabilities.
8. L. HE and W. NING 1998 *Unsteady Aerodynamics and Aeroelasticity of Turbomachines, Proceedings of the Eighth International Symposium, Stockholm, Sweden*, September 14–18, 183–189. Nonlinear harmonic analysis of unsteady transonic inviscid and viscous flows.
9. R. KIELB 2000 *The Nineth International Symposium of Unsteady Aerodynamics and Aeroelasticity of Turbomachines, Book of Abstracts. Lyon, France, September* 4–8. CFD for turbomachinery unsteady flows: an aeroelastic design perspective.
10. V. I. GNESIN and R. RZĄDKOWSKI 2000 *Transaction of the Institute of Fluid-Flow Machinery* **106**, 45–68. The theoretical model of 3D flutter in subsonic, transonic and supersonic inviscid flow.
11. R. RZĄDKOWSKI, V. GNESIN, V. and A. KOVALYOV 1997 *The Eighth International Symposium of Unsteady Aerodynamics and Aeroelasticity of Turbomachines, Stockholm, Sweden*, September 14–18, 317–334. The 2D flutter of bladed disc in an incompressible flow.
12. M. VAHDATI, A. I. SAYMA, L. SBARDELLA, J. G. MARSAHL and M. IMREGUN 2000 *The Nineth International Symposium of Unsteady Aerodynamics and Aeroelasticity of Turbomachines, Book of Abstracts, Lyon, France, September* 4–8. Ranking of numerical methods for fan flutter prediction.
13. R. RZĄDKOWSKI 1998 *Dynamics of Steam Turbine Blading, Part Two Bladed Discs.* Wrocław-Warszawa: Ossolineum.
14. R. RZĄDKOWSKI and V. I. GNESIN 2000 *Transaction of the Institute of Fluid-Flow Machinery* **106**, 69–95. The numerical and experimental verification of the 3D inviscid code.